Available online at www.sciencedirect.com
SCIENCE DIRECT®
Thin Solid Films 447–448 (2004) 201–207
thin solid films
www.elsevier.com/locate/tsf

# Mechanical and optical properties of hard SiCN coatings prepared by PECVD

P. Jedrzejowski[a], J. Cizek[b], A. Amassian[a], J.E. Klemberg-Sapieha[a,*], J. Vlcek[b], L. Martinu[a]

[a]*Groupe de recherche en physique et technologie des couches minces (GCM) and Department of Engineering Physics, Ecole Polytechnique, 2900, boul. Edouard-Montpetit, Montreal, Quebec, Canada, H3C 3A7*
[b]*Department of Physics, University of West Bohemia, Univerzitni 22, Plzen 306 14, Czech Republic*

**Abstract**

Novel amorphous SiCN coatings are becoming increasingly attractive because of their mechanical, optical and electronic properties. In the present work, SiCN films were fabricated by PECVD from $SiH_4/CH_4/N_2/Ar$ gas mixtures at a temperature of 400 °C. Mechanical properties such as hardness, Young's modulus, friction coefficient and stress were evaluated, respectively, by depth-sensing indentation, pin-on-disk, micro-scratch and curvature methods. Films deposited under optimized conditions exhibited a hardness >30 GPa, Young's modulus >190 GPa, elastic rebound of 85% and a compressive stress of approximately 1 GPa. A friction coefficient against $Al_2O_3$, ranging from 0.75 to 0.25 and a low surface roughness of approximately 1 nm were found to be accompanied by a refractive index ranging from 1.85 to 2.10 (at 550 nm) and an extinction coefficient between $1.0\times10^{-4}$ and $4.5\times10^{-2}$. The film behavior is correlated with the microstructure and composition determined by SEM, XPS, AFM and broad-range UV–VIS–NIR–IR spectroscopic ellipsometry.


*Keywords:* PECVD; SiCN; Mechanical properties; Spectroscopic ellipsometry; Microstructure

## 1. Introduction

In recent years, ternary silicon carbon nitrides (SiCN) have attracted considerable interest due to their exceptional mechanical, tribological and optical properties. Chemical inertness and high hardness [1–4] make SiCN ceramics a promising option for new micro-electromechanical systems (MEMS) [5]. Good wetting behavior [6], attractive tribological properties [7] and high temperature oxidation resistance [8] offer many other applications in coating technologies. 'Tunable' band gap characteristics (band gap engineering) [1,9,10], adjustable transparency in the visible and IR regions [11–13] and high thermal stability [14] make them attractive for microelectronics and optoelectronics.

SiCN can be formed by combining binary materials, such as $SiN_{1.3}$, SiC and CN. Each of these three materials provides the following intrinsic property: $SiN_{1.3}$ is a highly transparent, wide band gap (approx. 5 eV) dielectric [15,16]. SiC possesses a lower band gap (approx. 2.8 eV) and is characterized by excellent mechanical performance [16,17] and CN contributes high hardness, partial electrical conductivity and high elastic rebound [18] due to a fullerene-like microstructure [19]. These three materials form solid solution [20]. Therefore, by changing the phase content and by controlling the short range order it is possible to tune the properties of SiCN films to specific applications. In addition, this ternary material also possesses a complex chemical structure containing Si, C and N.

SiCN films have been prepared by various techniques, which include: pyrolysis of polymer precursors [8], chemical vapor deposition (CVD) at elevated temperatures [2], bias-assisted hot filament CVD [21], radio frequency plasma-enhanced CVD (PECVD) [22,23], microwave PECVD [24,25], electron cyclotron resonance PECVD [9–11], pulsed laser deposition [4,12], ion beam sputtering [3,26] and reactive magnetron sputtering [6,27,28].

Although, many significant and encouraging results have been reported on ternary SiCN films, optimization of the optical and mechanical performance and micro-

*Corresponding author. Tel.: +1-514-340-5747; fax: +1-514-340-3218.
*E-mail address:* jsapieha@polymtl.ca (J.E. Klemberg-Sapieha).

0040-6090/04/$ - see front matter © 2003 Elsevier B.V. All rights reserved.
doi:10.1016/S0040-6090(03)01057-5

structure has not yet been fully explored. PECVD technique offers an attractive opportunity to fabricate amorphous hydrogenated SiCN films at intermediate substrate temperatures and it provides high quality films with good adhesion, good coverage of complicated substrate shapes and high deposition rate. In the present work, we specifically focus on the correlation between process parameters, structure, mechanical, tribological and optical properties of these films. Our methodological approach is based on the enhancement of the mechanical properties of $SiN_{1.3}$ by adding $CN_x$ and SiC components in anticipation of obtaining a hard material with a wide band gap and with suitable optical and electronic characteristics.

## 2. Experimental methodology

### 2.1. Film deposition

SiCN films were deposited in a radio frequency (RF, 13.56 MHz) plasma system in which the substrates were held on an RF powered electrode (15 cm in diameter). An RF-induced negative DC self-bias, $V_B$, developed on the electrode. The substrate holder was heated to 400 °C using halogen lamps. $SiH_4$, $CH_4$, $N_2$ and Ar working gases were introduced via circular distributors. Their flow was controlled by MKS mass-flow controllers in each line and the working pressure was measured by a capacitance gauge (MKS Baratron). Prior to deposition, the system was evacuated to $10^{-3}$ Pa using a turbomolecular pump.

The film fabrication process consisted of two plasma pretreatment steps in Ar and in $N_2$ for 10 and 20 min, respectively, followed by a 1.5 h long deposition using the conditions summarized in Table 1. The choice of process parameters resulted from a preliminary optimization study, which obtained high quality $SiN_{1.3}$ with respect to its optical and mechanical properties [15]. In all depositions, the conditions were held constant, while the concentration of carbon (C) in $SiN_{1.3}$ was controlled by adjusting the flow of $CH_4$ ($F_{CH4}$) between 0 sccm (pure $SiN_{1.3}$) and 60 sccm. Film thickness, measured by Sloan Dektak II profilometer and a variable angle spectroscopic ellipsometer (VASE, J.A. Woollam Co.) was between 1.0 and 1.5 μm. Based on our earlier studies of ion fluxes and ion energy distribution functions in the same reactor [29], we estimated that the ion current density during the film growth was approximately 150 $\mu A/cm^2$. Crystalline silicon (c-Si) (100) was used as substrate and was cleaned prior to deposition in an ultrasonic bath with acetone and isopropanol to eliminate organic surface contaminants.

### 2.2. Composition characterization

Chemical composition and chemical structure were analyzed, respectively, by X-ray photoelectron spectroscopy (XPS) and infrared variable angle spectroscopic ellipsometry (IR VASE). XPS analysis was carried out in a VG ESCALAB 3 Mark II instrument with a non-monochromated $MgK_\alpha$ source (1256.6 eV) with a 0.8 eV resolution. The IR VASE spectra were measured between 2.5 and 34 μm (i.e. approx. from 4000 to 220 $cm^{-1}$) using 5 angles of incidence between 65 and 75°. Similar to VIS VASE, these measurements were taken in reflection; therefore, the influence of substrate absorption, which is a critical factor in standard FTIR spectroscopy, was eliminated. Contrary to FTIR measurements, IR VASE (and ellipsometry in general) did not directly measure the absorption coefficient $\alpha$, but it was determined from a simulation of the optical behavior in the IR region. The physical model used for IR VASE data consisted of a c-Si substrate with a native $SiO_2$ layer, 3 nm thick, a 'general oscillator' and a surface roughness layer. In the 'general oscillator' model, interband absorptions were simulated by Lorentz-type oscillators; their parameters were found using the Levenberg–Marquardt algorithm during a fitting procedure. In addition, inhomogeneities in the optical constants throughout the film thickness were modeled by 'mixing' the optical response of the pure material with voids. Detected inhomogeneities were not larger than 10%. Film morphology was also assessed by scanning electron microscopy (SEM, Philips XL 20) and by Atomic Force Microscopy (AFM, Digital Instruments, $2\times2$ μm scanned surface).

### 2.3. Optical and mechanical properties

The refractive index, $n$, and extinction coefficient, $k$, were determined by VASE in the visible (VIS) and near infrared (NIR) regions between 300 and 1600 nm using angles of incidence of 55°, 65° and 75°. The optical

Table 1
Deposition conditions for PECVD SiCN films

| Process | Time (min) | Substrate temperature (°C) | Pressure (Pa) | Bias voltage (V) | Gas flow (sccm) | | | |
|---|---|---|---|---|---|---|---|---|
| | | | | | Ar | $N_2$ | $SiH_4$ | $CH_4$ |
| Pretreatment (1) | 10 | 400 | 7 | –600 | 60 | – | – | – |
| Pretreatment (2) | 30 | 400 | 7 | –600 | 10 | 25 | – | – |
| Deposition of SiCN | 90 | 400 | 13 | –600 | 8 | 35 | 5 | 0–60 |

data were fitted using the WVASE software (J.A. Woollam Co. Inc.) and the same model as for IR VASE.

The hardness, $H$, and reduced Young's modulus, $E_r$, were assessed by depth-sensing indentation using a Triboindenter (Hysitron Inc.) equipped with a Berkovich pyramid and using the Oliver and Pharr [30] method for data analysis. Since, the methodology of mechanical testing of very hard films with a pronounced elastic response is controversial, we performed a detailed analysis of the depth-sensing indentation procedure [31]. This included evaluation of the effects of indentation load, depth of penetration and assessment of the indenter area function. The results presented in this work were obtained from 10 indentations using a load ranging from 3 to 10 mN.

Film stress was obtained from the curvature of silicon substrates before and after deposition, using a Sloan DEKTAK II profilometer and the Stoney formula [32]. The stress measurements were performed on silicon wafer stripes, which were 30 mm long, 5 mm wide and 0.3 mm thick. The friction coefficient, $\mu$, at room temperature (approx. 25 °C) and a relative humidity of approximately 55% was evaluated using pin-on-disc tribometer and micro-scratch tester (CSEM, Neuchatel). The tribometer was equipped with a 6 mm diameter $Al_2O_3$ ball. In all experiments, the applied load was 0.25 N and the sliding speed was 10 cm $s^{-1}$. The values of $\mu$ reported here refer to the steady-state conditions. In all cases, the travelled distance was greater than 50 m. The micro-scratch tester was equipped with a 200 μm radius Rockwell C diamond stylus. The applied load was 1 N and $\mu$ was measured along a distance of 10 mm.

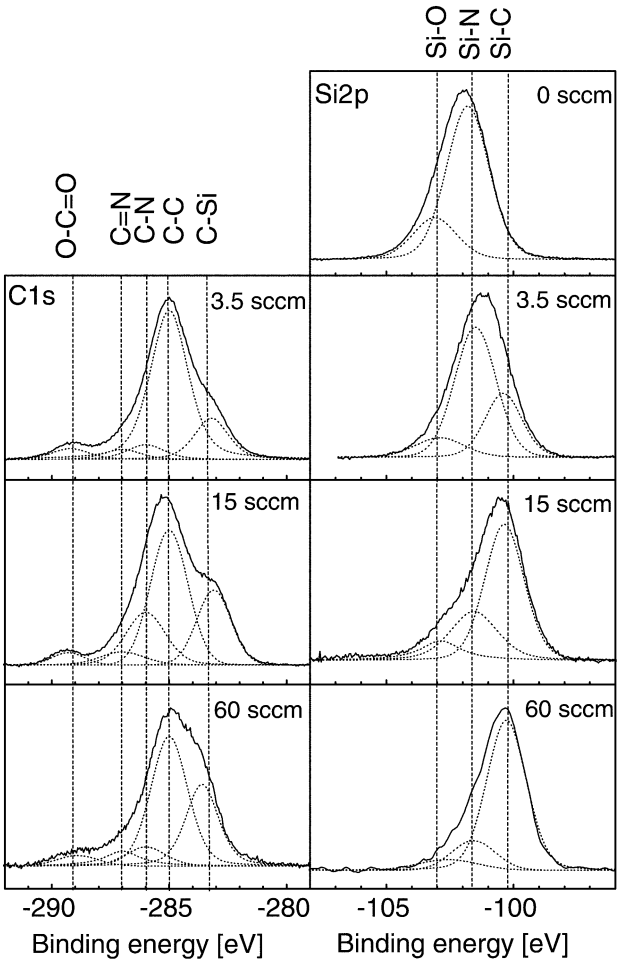


Fig. 1. High resolution XPS spectra of C1s and Si2p core levels for $CH_4$ gas flows of 0, 3.5, 15 and 60 sccm.

## 3. Results and discussion

### 3.1. Structural characterization

The results of XPS compositional analysis are shown in Table 2. The high-resolution XPS spectra of C1s and Si2p core level peaks are presented in Fig. 1 and Table 3 for pure $SiN_{1.3}$ and SiCN with different $F_{CH4}$. The Si2p spectrum for pure $SiN_{1.3}$ showed a presence of Si–N bonds at 101.6 eV and the contribution of Si–$O_x$ bonds at 103.0 eV due to surface contamination. When $CH_4$ was added, the Si–C bond at 100.4 eV appeared. The C1s spectrum for SiCN was deconvoluted into five components due to C–Si at 283.4 eV, C–C or C–H at 285.0 eV, C–N at 286.0 eV (C–O was also possible), C=N at 287.0 eV (C=O was also possible) and O–C=O at 289.0 eV chemical bonds [33]. The N1s spectrum at 397.6–400.2 eV exhibited a broad peak, difficult to deconvolute due to overlapping of different N- containing groups (not shown here).

Complementary information about the chemical structure was obtained from IR VASE measurements. Examples of deconvoluted absorption spectra for $F_{CH4}=0$, 0.75 and 60 sccm are presented in Fig. 2. Assignment of the absorption bands was based on literature data [16,20,34–39] (see Table 4). The IR spectra in Fig. 2 revealed the main absorption region between 500 and 1500 $cm^{-1}$ due to the presence of Si–C, Si–H, Si–N and N–H bonds. The relative intensity of these peaks varied with $F_{CH4}$. Due to the amorphous structure and a

Table 2
Elemental composition measured by XPS

| $CH_4$ flow (sccm) | Elemental composition (at.%) | | | |
|---|---|---|---|---|
| | Si | N | C | O |
| 0 | 37.1 | 45.9 | 9.0 | 8.0 |
| 0.75 | 30.8 | 37.6 | 21.0 | 10.6 |
| 3.5 | 34.9 | 28.0 | 25.6 | 11.5 |
| 7.0 | 31.2 | 32.6 | 27.0 | 9.2 |
| 15 | 25.1 | 38.1 | 28.0 | 7.8 |
| 30 | 31.0 | 25.8 | 31.2 | 12.0 |
| 60 | 32.0 | 22.0 | 35.0 | 11.0 |

Table 3
Peak position and area of deconvoluted C1s and Si2p peaks for $SiN_{1.3}$ and SiCN

| $CH_4$ flow (sccm) | Peak: C1s (eV) | | | | | Peak: Si2p (eV) | | |
|---|---|---|---|---|---|---|---|---|
| | C–Si 283.2–283.4 | C–C 285.0 | C–O C–N 286.0 | C=O C=N 287.0 | O–C=O 289.0 | Si–C 100.4 | Si–N 101.6–101.8 | Si–O 103.0 |
| 0 | | 86.0 | 8.6 | 2.2 | 3.2 | | 79.6 | 20.4 |
| 0.75 | 6.5 | 71.9 | 6.6 | 7.0 | | 11.6 | 82.1 | 6.3 |
| 3.5 | 18.7 | 61.1 | 10.0 | 5.4 | 4.8 | 24.8 | 62.2 | 14.5 |
| 7.0 | 20.9 | 59.1 | 12.0 | 3.0 | 5.0 | 35.8 | 61.3 | 2.9 |
| 15 | 25.0 | 47.6 | 17.8 | 5.3 | 4.3 | 52.3 | 41.0 | 6.7 |
| 30 | 28.2 | 53.7 | 8.0 | 4.4 | 5.7 | 58.2 | 37.2 | 4.6 |
| 60 | 30.2 | 52.5 | 7.0 | 5.1 | 5.2 | 62.8 | 33.8 | 3.4 |

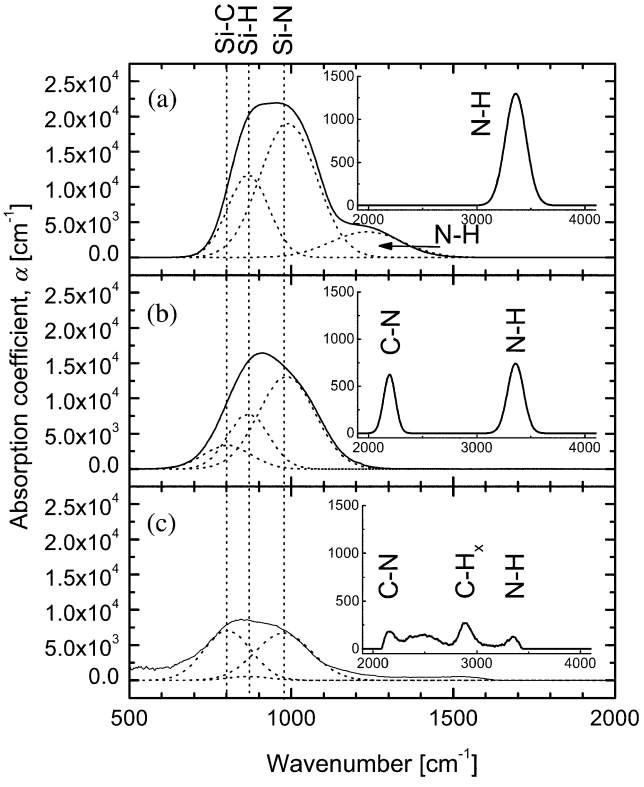


Fig. 2. IR spectra obtained by IR VASE for 0 sccm of $CH_4$ (a), 3.5 sccm of $CH_4$ (b) and 60 sccm of $CH_4$ (c).

Table 4
Position of IR absorption peaks

| Bonding | Wavenumber ($cm^{-1}$) |
|---|---|
| Si–C | ~800 |
| Si–H | ~870 |
| Si–N | 975–990 |
| N–H | ~1233 |
| C–N | ~2200 |
| $C–H_x$ | ~2900 |
| N–H | ~3400 |

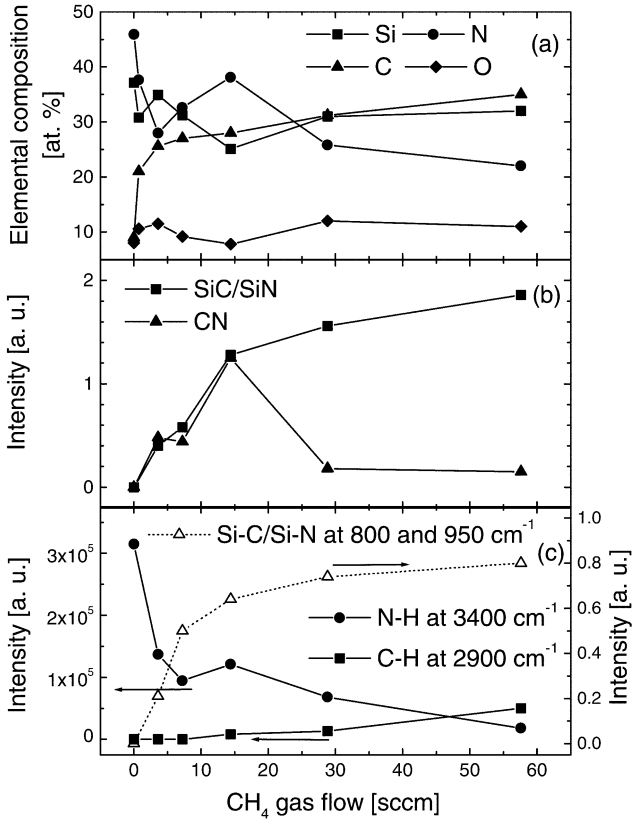


Fig. 3. The effect of $CH_4$ flow on the elemental composition (a), on the peak intensities due to CN bonds and SiC/SiN phase ratio obtained by XPS (b), and on the IR absorption peak intensity for N–H and $C–H_x$ bonds and for the SiC/SiN bond concentration ratios measured by IR VASE (c).

complex short range order chemical environment, the main Si–N absorption peak was relatively large. The Si–C/Si–N ratio increased and the main peak shifted towards lower wavenumbers.

The data obtained from the IR VASE and XPS measurements are summarized in Fig. 3. The effect of $F_{CH4}$ added to the gas mixture on the surface composition is presented in Table 2 and in Fig. 3a. C content

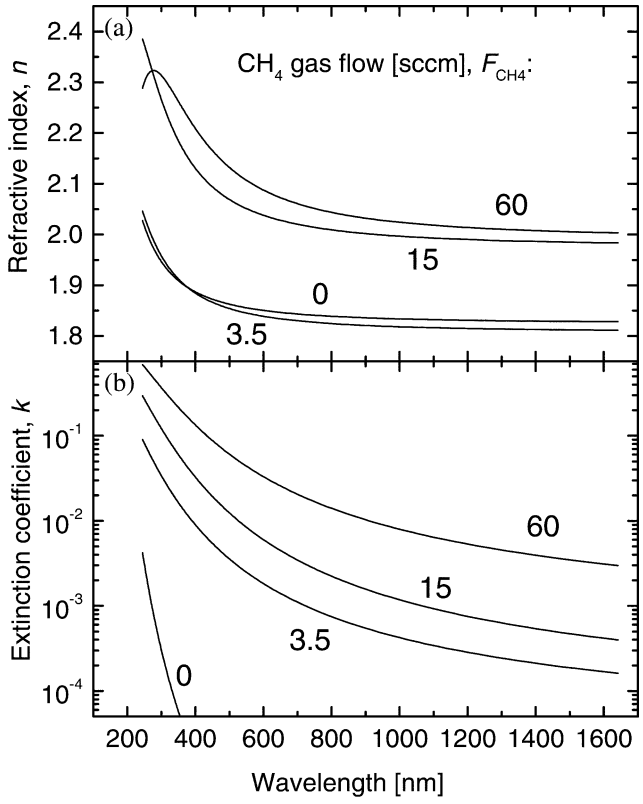


Fig. 4. Refractive index (a) and extinction coefficient (b) as a function of $CH_4$ gas flow.

steadily increased, while Si and N content fluctuated with a tendency to decrease. We estimated that at least 9 at.% of C was due to adventitious hydrocarbon, while surface contamination by O was approximately 8–10 at.%.

Both techniques indicated that increasing $F_{CH4}$ gave rise to a steadily increasing Si–C/Si–N ratio. This suggested that C substituted for N in the chemical structure of SiCN. The CN phase content increased with $F_{CH4}$ up to 15 sccm, but it decreased for higher flow rate values. This was accompanied by an appearance of C–$H_x$ bonds and a steady decrease of N–H bonds (Fig. 3c), indicating that additional carbon contributed to the formation of C–$H_x$ bonds rather than C–N bonds.

All samples studied in this work were found to be amorphous and densely packed as confirmed by the featureless SEM cross-section observations. Direct measurement of the film thickness confirmed the data obtained by VASE. Surface roughness, $R_a$, was found to be approximately 1 nm, thus confirming a very smooth surface of PECVD amorphous films.

### 3.2. Optical and mechanical properties

Examples of dispersion curves of SiCN films obtained from VASE measurements in the UV–VIS–NIR regions

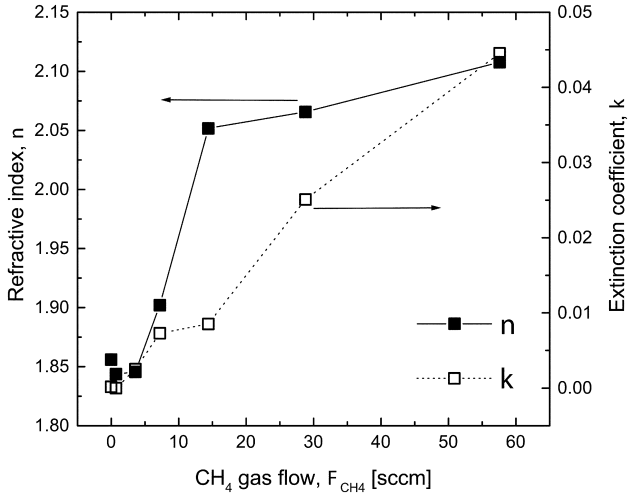


Fig. 5. Refractive index and extinction coefficient at 550 nm as a function of $CH_4$ gas flow.

are shown in Fig. 4 for the films deposited with increasing $F_{CH4}$ and hence, C. For low $F_{CH4}$ ($<3.5$ sccm), the $n(\lambda)$ curves are very similar. For $F_{CH4}>3.5$ sccm, $n$ and $k$ increase, an effect which can be attributed to the presence of SiC and CN bonds ($n\sim2.50$, 2.60 and 1.85 for SiC, CN and $SiN_{1.3}$, respectively). The $n$ and $k$ values at $\lambda=550$ nm are shown plotted in Fig. 5. The increase of $n$ from 1.85 to 2.10 is accompanied by an increase of $k$ from $10^{-4}$ to $4\times10^{-2}$. The increase in absorption can be attributed to the presence of carbon that is bonded neither to Si nor to N (as observed by IR VASE).

Fig. 6 presents a comparison of the load displacement curves obtained for $SiN_{1.3}$ and for SiCN that exhibits the highest $H$ and $E_r$ values. The shape of the curve clearly points to high elastic properties of the SiCN films. By calculating the ratio of the area between the

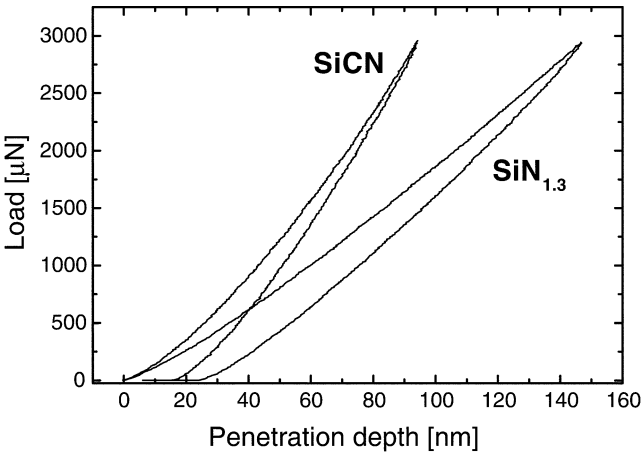


Fig. 6. Examples of load–displacement curves for pure $SiN_{1.3}$ and for SiCN with $H=33$ GPa.

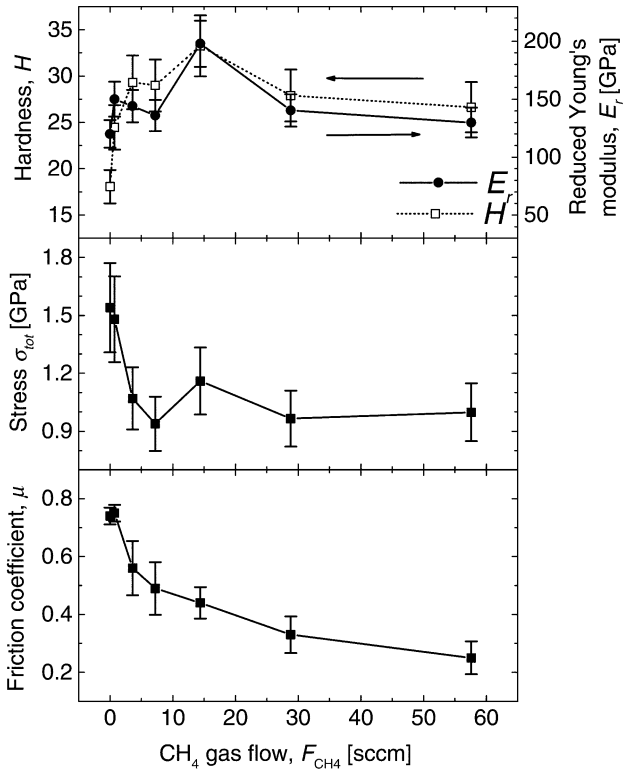


Fig. 7. The effect of $CH_4$ gas flow on the hardness and reduced Young's modulus (a), total compressive stress (b), and the friction coefficient (c).

loading and unloading curves (elastic deformation) to the area below the loading curve (plastic deformation), we obtain the elastic recovery, $R$. For the SiCN curve in Fig. 6, $R \sim 85\%$.

The effect of $F_{CH4}$ on the evolution of the mechanical properties is shown in Fig. 7. Both $H$ and $E_r$ dependences (Fig. 7a) exhibit a similar behavior; they increase with increasing $F_{CH4}$ from 18 and 120 GPa for pure $SiN_{1.3}$, up to 33 and 200 GPa at $F_{CH4}=15$ sccm, respectively. Further increase of $F_{CH4}$ leads to a decrease of $H$ and $E_r$.

In general, SiC and CN are materials possessing high $H$ and $E$ values. They may reach $\sim 26$, $\sim 480$ GPa and $\sim 60$ and $\sim 250$ GPa, respectively, for SiC and CN [19,32]. Adding C to $SiN_{1.3}$ led to the creation of C–Si and C–N bonds and increased both $H$ and $E_r$ to a maximum value at the optimum $F_{CH4}$. At $F_{CH4}=15$ sccm, the phase composition was characterized by the highest amount of CN phase (see Fig. 3b). Increase of C beyond this value led to the creation of $CH_x$ groups (see Fig. 3a), which decreased $H$ and $E_r$.

Increasing $F_{CH4}$ led to a monotonic decrease of $\sigma_{tot}$ from $-1.5$ GPa to $-1.0$ GPa, as presented in Fig. 7b. In this figure, the value of $\sigma_{tot}$ is the sum of the intrinsic stress, $\sigma_{int}$, and the thermal stress, $\sigma_{th}$ ($\sigma_{tot}=\sigma_{int}+\sigma_{th}$). In order to separate $\sigma_{int}$, we calculated $\sigma_{th}$ by approximating the coefficient of thermal expansion (CTE) for SiCN by the CTE for pure $SiN_{1.3}$ ($3.3\times10^{-6}$ $K^{-1}$) and for the c-Si substrate ($4.1\times10^{-6}$ $K^{-1}$) [32]. In this case, $\sigma_{th}$ was compressive ($\sigma_{th}=-0.1$ GPa) and small compared to $\sigma_{tot}$. The stress in PECVD films was low compared to their PVD equivalents, for which $\sigma_{tot}>2$ GPa has been reported [40]. This could be attributed to a lower ion bombardment energy and lower ion current intensity during the PECVD deposition process. For a typical RF discharge at approximately 13 Pa, the $Ar^+$ ion energies are in the range of 100 eV when using the power levels described in this work [29].

The effect of $F_{CH4}$ on $\mu$ is shown plotted in Fig. 7c. The values of $\mu$ monotonically decreased from 0.75 to 0.25. This could be related to an increasing concentration of C–C bonds that rendered the surface more lubricious [41]. Similar values measured under the same conditions were found for PVD SiCN films for C ranging from 6 to 60 at.% [27]. For comparison, $\mu$ measured by the micro-scratch tester using a diamond stylus was found to be very small (between 0.04 and 0.06) and constant with $F_{CH4}$. This low value clearly resulted from the low friction coefficient of diamond.

## 4. Conclusions

We systematically studied the composition, and the mechanical and optical properties of amorphous SiCN films in which the carbon content was sequentially varied from 0 to 35 at.%. For an optimum $F_{CH4}=15$ sccm, that corresponds to 28 at.% of C, we obtained the highest values of hardness and Young's modulus (33 and 200 GPa, respectively). These films were characterized by a high elastic rebound of $\sim 85\%$, low compressive stress of $\sim 1.1$ GPa, low surface roughness $R_a \sim 1$ nm and a friction coefficient of 0.4. Through the control of the film's composition, we were able to vary the refractive index and the extinction coefficient (at 550 nm) from 1.85 to 2.10 and from $1.0\times10^{-4}$ to $4.5\times10^{-2}$, respectively. The 'optimum' properties correspond to the composition of 25 at.% Si, 38 at.% N and 28 at.% C associated with the SiN, CN and SiC bonding as determined by XPS, and broad range UV–VIS–NIR-IR spectroscopic ellipsometry. Future work will be directed to the implementation of SiCN in the thin film systems for electronic, optoelectronic and tribomechanical devices.

## Acknowledgments

The authors acknowledge the expert technical assistance of Mr Jiri Cerny and Mr Gilles Jalbert. We also wish to thank Dr Oleg Zabeida, Dr Jorg Oberste-Berghaus and other members of the GCM for stimulating discussions. This work was supported by the Natural Sciences and Engineering Research Council (NSERC)

of Canada and by the Ministry of Education of the Czech Republic (Project No. MSM 235200002).

## References

[1] A. Badzian, T. Badzian, R. Roy, W. Drawl, Thin Solid Films 354 (1999) 148.
[2] A. Bendeddouche, R. Berjoan, E. Beche, R. Hillel, Surf. Coat. Technol. 111 (1999) 184.
[3] Z. He, G. Carter, J.S. Colligon, Thin Solid Films 283 (1996) 90.
[4] T. Thärigen, G. Lippold, V. Riede, M. Lorenz, K.J. Koivusaari, D. Lorenz, S. Mosch, P. Grau, R. Hesse, P. Streubel, R. Szargan, Thin Solid Films 348 (1999) 103.
[5] L.-A. Liew, Y. Liu, R. Luo, T. Cross, L. An, V.M. Bright, M.L. Dunn, J.W. Daily, R. Raj, Sens. Actuat. A 95 (2002) 120.
[6] T. Berlind, N. Hellgren, M.P. Johansson, L. Hultman, Surf. Coat. Technol. 141 (2001) 145.
[7] E. Bertran, E. Martínez, G. Viera, J. Farjas, P. Roura, Diamond Relat. Mater. 10 (2001) 1115.
[8] R. Riedel, H.-J. Kleebe, H. Schönfelder, F. Aldinger, Nature 374 (1995) 526.
[9] D.H. Zhang, Y. Gao, J. Wei, Z.Q. Mo, Thin Solid Films 377–378 (2000) 607.
[10] K.H. Chen, J.-J. Wu, C.Y. Wen, L.C. Chen, C.W. Fan, P.F. Kuo, Y.F. Chen, Y.S. Huang, Thin Solid Films 355–356 (1999) 205.
[11] F.J. Gómez, P. Prieto, E. Elizalde, J. Piquerasa, Appl. Phys. Lett. 69 (1996) 773.
[12] G. Soto, E.C. Samano, R. Machorro, L. Cota, J. Vac. Sci. Technol. A16 (1998) 1311.
[13] L.C. Chen, H.Y. Lin, C.S. Wong, K.H. Chen, S.T. Lin, Y.C. Yu, C.W. Wang, E.K. Lin, K.C. Ling, Diamond Relat. Mater. 8 (1999) 618.
[14] H.J. Seifert, J. Peng, H.L. Lukas, F. Aldinger, J. Alloys Compd. 320 (2001) 251.
[15] R. Vernhes, O. Zabeida, J.E. Klemberg-Sapieha, L. Martinu, Appl. Opt. 2003, submitted.
[16] K.B. Sundaram, J. Alizadeh, Thin Solid Films 370 (2000) 151.
[17] M.A. El Khakani, M. Chaker, A. Jean, S. Boily, J.C. Kieffer, M.E. O'Hern, M.F. Ravet, F. Rousseaux, J. Mater. Res. 9 (1994) 96.
[18] V. Hajek, K. Rusnak, J. Vlcek, L. Martinu, S.C. Gujrathi, J. Vac. Sci. Technol. A17 (1999) 899.
[19] H. Sjostrom, L. Hultman, J.-E. Sundgren, S.V. Hainsworth, T.F. Page, G.S.A.M. Theunissen, J. Vac. Sci. Technol. A14 (1996) 56.
[20] Y. Gao, J. Wei, D.H. Zhang, Z.Q. Mo, P. Hing, X. Shi, Thin Solid Films 377–378 (2000) 562.
[21] Z. Gong, E.G. Wang, G.C. Xu, Y. Chen, Thin Solid Films 348 (1999) 114.
[22] H. Sachdev, P. Scheid, Diamond Relat. Mater. 10 (2001) 1160.
[23] G. Viera, J.L. Andújar, S.N. Sharma, E. Bertran, Diamond Relat. Mater. 7 (1998) 407.
[24] L.C. Chen, C.Y. Yang, D.M. Bhusari, K.H. Chen, M.C. Lin, J.C. Lin, T.J. Chuang, Diamond Relat. Mater. 5 (1996) 514.
[25] J.-Y. Wu, C.-T. Kuo, P.-J. Yang, Mater. Chem. Phys. 72 (2001) 245.
[26] J.-J. Wu, C.-T. Wu, Y.-C. Liao, T.-R. Lu, L.C. Chen, K.H. Chen, L.-G. Hwa, C.-T. Kuo, K.-J. Ling, Thin Solid Films 355–356 (1999) 417.
[27] J. Vlček, M. Kormunda, J. Čízek, V. Peřina, J. Zemek, Surf. Coat. Technol. 160 (2002) 74.
[28] H. Lutz, M. Bruns, F. Link, H. Baumann, Thin Solid Films 332 (1998) 230.
[29] A. Hallil, O. Zabeida, M.R. Wertheimer, L. Martinu, J. Vac. Sci. Technol. A18 (2000) 882.
[30] W.C. Oliver, G.M. Pharr, J. Mater. Res. 7 (1992) 1564.
[31] P. Jedrzejowski, J.E. Klemberg-Sapieha, L. Martinu, Thin Solid Films 426 (2003) 150.
[32] M. Ohring, The Materials Science of Thin Films, Plenum Press, New York, 1992, p. 418, 552.
[33] J.F. Moulder, W.F. Stickle, P.E. Sobol, K.D. Boniber, in: J. Chastain (Ed.), Handbook of X-Ray Photoelectron Spectroscopy, Perkin-Elmer, Eden Prairie, MN, 1992, p. 29.
[34] A.M. Wrobel, A. Walkiewicz-Pietrzykowska, J.E. Klemberg-Sapieha, Y. Hatanaka, T. Aouki, Y. Nakanishi, J. Appl. Polym. Sci. 86 (2002) 1445.
[35] X.-C. Xiao, Y.-W. Li, L.-X. Song, X.-F. Peng, X.-F. Hu, Appl. Surf. Sci. 156 (2000) 155.
[36] J. Schuhmacher, F. Berger, M. Weinmann, J. Bill, F. Aldinger, K. Muller, Appl. Organomet. Chem. 15 (2001) 809.
[37] S. Ulrich, H. Ehrhardt, T. Theel, J. Schwan, S. Westermeyr, M. Scheib, P. Becker, H. Oechsner, G. Dollinger, A. Bergmaier, Diamond Relat. Mater. 7 (1998) 839.
[38] X. Peng, L. Song, J. Le, X. Hu, J. Vac. Sci. Technol. B 20 (2002) 159.
[39] W.S. Liao, C.H. Lin, S.C. Lee, Appl. Phys. Lett. 65 (1994) 2229.
[40] M. Lattemann, S. Ulrich, H. Holleck, A. Stuber, H. Leiste, Diamond Relat. Mater. 11 (2002) 1248.
[41] K. Holmberg, A. Matthews, Coatings Tribology: Properties, Techniques and Applications in Surface Engineering, Elsevier, 1994, p. 209.